Laser Photonics Rev. **7,** No. 5, L51–L54 (2013) / **DOI** 10.1002/lpor.201300042

LASER & PHOTONICS REVIEWS

A new form of induced transparency enabled by dynamical tunneling coupling of continuous chaos and discrete regular modes in a slightly deformed optical microcavity is demonstrated experimentally. An optical beam is focused on the cavity boundary and tuned on resonance with a high-Q mode, which leads to destructive interference for the excitation of chaotic field and induces a transparency in the transmission. The experimental results are in excellent agreement with a model based on quantum scattering theory. This tunneling-induced transparency is accompanied by extremely steep normal dispersion, and holds great potential in slow light and enhanced nonlinear interactions.

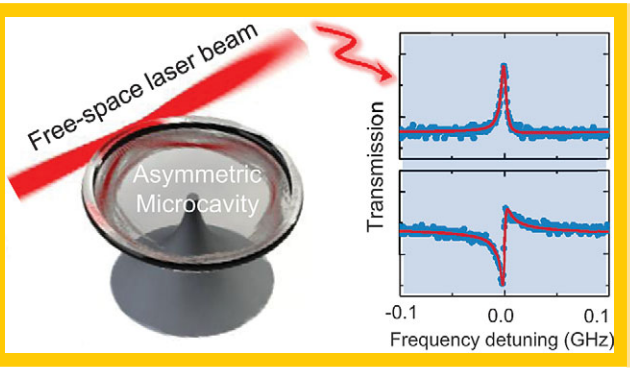

LETTER ARTICLE

Tunneling-induced transparency in a chaotic microcavity

Yun-Feng Xiao*, Xue-Feng Jiang, Qi-Fan Yang, Li Wang, Kebin Shi, Yan Li, and Qihuang Gong*

An opaque atomic medium can be made transparent in the presence of a strong control laser beam, in a process known as electromagnetically induced transparency (EIT) [1]. EIT has led to novel concepts and important consequences, such as light freezing, enhanced nonlinear interactions and lasing without inversion [2]. These have put EIT to the forefront of experimental study in atomic physics during the last two decades. It has been recently recognized and demonstrated that similar interference effects occur in linear classical systems such as plasma [3, 4], electric circuits [5, 6], photonic microresonators [7–11], metamaterials [12, 13] and optomechanical systems [14, 15], which bring the original quantum phenomenon into the realm of classical optics. Remarkably, this all-optical form of induced transparency does not require naturally occurring resonances and can therefore be applied to previously inaccessible wavelength regions. Equally importantly, no strong pumping is required. In this Letter, we experimentally demonstrate a new form of induced transparency in a slightly deformed microcavity, in which the ray dynamics result in a mixed phase space including both regular and chaotic trajectories [16–19]. The induced transparency originates from dynamical tunneling between the regular and the chaos [20], so it is termed as *tunneling-induced transparency*.

Figure 1(a) depicts the coupled system in which a deformed toroidal microcavity is excited by a free-space laser beam focused on the cavity boundary. The boundary of the microtoroid is defined as $r(\phi) = r_0(1 + \sum_{i=2,3} a_i \cos^i \phi)$ for $\cos\phi \geq 0$, and $r_0(1 + \sum_{i=2,3} b_i \cos^i \phi)$ for $\cos\phi < 0$ in the polar coordinates (r, ϕ), where r_0 denotes the size parameter. The deformed microcavity was constructed by combining a two-step dry etching and a CO_2 pulse laser irradiation, described elsewhere [21,22]. In our experiment, the resulting microtoroid has geometrical parameters following the theoretical design of $r_0 \sim 45\ \mu$m, $a_2 \sim -0.133$, $a_3 \sim 0.095$, $b_2 \sim -0.064$, and $b_3 \sim -0.022$ (Ref. [22]). The thickness of the disk is 2 μm and the minor radius of the toroid is 2.5 μm, which means that the inner walls raised by the toroid cast little influence on the transportation of light into the disk part, different from the annular microcavities [23] and the ring resonantors [24]. The deformed microtoroid supports resonances with both ultrahigh Q factors and highly directional emission toward the 180° far-field direction (emitted at polar angle positions $\phi \sim \pi/2$ and $3\pi/2$) [22], as shown in red in Fig. 1(a).

A consequence of the aforementioned directional emission is that time-reversing the process enables excitation of high-Q resonances with a free-space beam [25, 26]. The whole interaction process is shown in Fig. 1(b), characterized by a three-level configuration: ground, chaos, and high-Q resonance. Throughout this paper, the concepts of regular mode and chaotic mode are used to describe uncoupled states, and dynamical tunneling can be treated as the interaction between an *uncoupled* regular mode and *uncoupled* chaotic modes [25]. In general, both direct tunneling and dynamical tunneling can excite the high-Q regular mode. To provide a better understanding, first, Fig. 1(c) (black) plots the phase space of the deformed microcavity. It is found that the ray dynamics is mostly chaotic, in addition to some regular orbits such as islands and Kalmogorov-Arnol'd-Moser (KAM) tori [27]. In ray optics, these different structures are disjoint; while in reality, dynamical tunneling takes place between the regular and neighboring chaotic orbits. The dynamical tunneling can be demonstrated by a Husimi

State Key Lab for Mesoscopic Physics, Department of Physics, Peking University, P. R. China
*Corresponding author(s): e-mail: yfxiao@pku.edu.cn; qhgong@pku.edu.cn

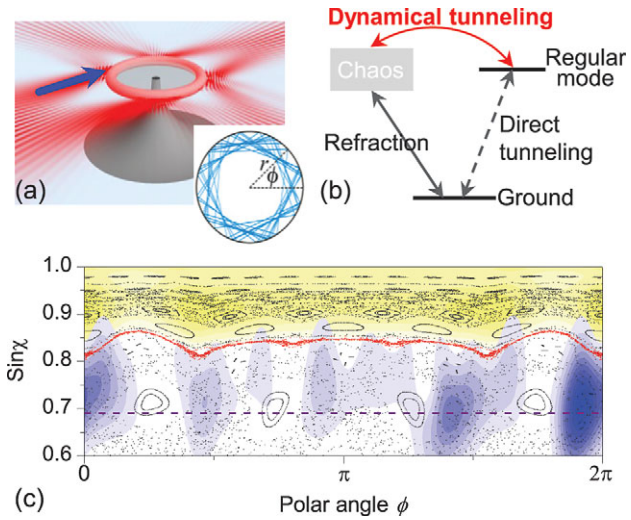

Figure 1 (a) Schematic illustration of a deformed silica microtoroid excited by a focused free-space laser beam (waist: 3 μm). The blue arrow indicates the excitation beam from the 180° far-field direction. The red plotting describes the spatial distribution of a high-Q resonance, where the field outside is magnified. Inset: real-space chaotic trajectories (blue curves) in the cavity. r, ϕ give the polar coordinate system in the cavity plane. (b) The schematic illustration of the interaction mechanism. (c) The phase-space structure for the deformed microcavity plotted in Birkhoff's coordinates. The red dotted curve above $\sin\chi = 0.8$ is a KAM torus, which divides the chaotic sea into classically accessible (bottom) and classically forbidden (upper) regions. The purple dashed curve at $\sin\chi = 0.69$ denotes the critical refraction line. Husimi distributions of the high-Q resonant field and the excitation field are shown in yellow and blue, respectively.

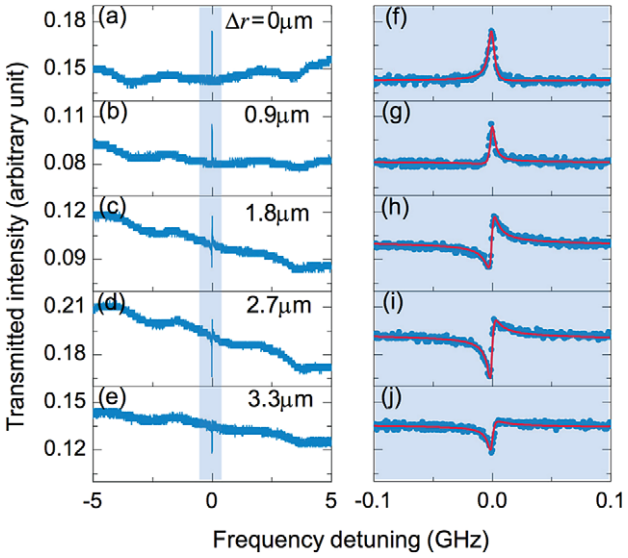

Figure 2 (a)–(e), Measured transmission spectra for different excitation positions of the focused beam. All figures have the same scales in both horizontal and vertical axes. From top to bottom, the focused beam moves away from the cavity boundary. The initial position ($\Delta r = 0$) is set to the highest induced transparency peak. (f)-(j) Zoom-in of the transmission spectra around the transparency window. Red solid curves correspond to model fits from Eq. (1).

projection (blue in Fig. 1(c)) of the excited chaotic field [17, 28], where some tails of the excitation field obviously intrude into the upper area by crossing the KAM torus. Second, the high-Q resonances in the deformed microcavity are located on the upper of the phase space (yellow in Fig. 1(c)), and their angular momenta have significant mismatch to the free-space beam focused on the cavity boundary. As a result, the direct tunneling is extremely weak, and the efficient excitation of high-Q resonances in the deformed microcavity is attributed to the dynamical tunneling. In this regard, finally, the EIT-like resonance in the free-space transmission spectrum can be understood by considering two excitation pathways: (1) direct excitation of the continuous chaos from the incident beam, and (2) excitation of the high-Q mode (by dynamical tunneling) coupling back to the chaos. Most importantly, these two pathways interfere destructively with each other because a phase shift occurs when light crosses the KAM torus which represents a potential barrier in the wave-optic field [29,30]. Thus, the cancellation of the chaos loss due to the destructive interference results in the induced transparency in the far transmitted field.

In the first experiment, the incident beam is injected from the 180° far-field direction and is focused to 3 μm in diameter with an objective lens (N.A.: 0.26) on the cavity edge at $\phi \sim \pi/2$. The transmitted light is collected in the 0° far-field direction by the other identical objective lens and finally enters into a photoreceiver. Figure 2(a) with the zoom-in (f) shows a typical power transmission spectrum for a quasi-TM resonance of the coupling system. A high-Q cavity resonance is observed to be excited in such a way that a sharp EIT phenomenon occurs. As the coupling position is moved away from the cavity boundary, this induced transparency experienced a transition to an asymmetric Fano resonance [31], as shown in Figs. 2 (b)-2(e) and 2(g)-2(j).

To further reveal the significance of free-space coupling, in our second experiment, a fiber taper is used to couple the same deformed cavity. Figures 3(a)–3(b) compare the transmission spectra obtained with the two methods. It can be seen that the high-Q resonance responses in both spectra show a good correspondence with a slight red shifting of the resonances when coupled to the taper. The target resonance mode has an intrinsic quality factor exceeding 3×10^7 at the wavelength of 1556.8 nm. The EIT-like characteristic in the free-space transmission spectrum differs from the symmetric Lorentzian dips. Moreover, no obvious change of the resonance lineshape is observed when the taper-cavity system is tuned continuously from under- to strongly over-coupled regions as Fig. 3(c). The principal difference between free-space coupling and taper coupling is that taper coupling directly excites high-Q regular modes within the cavity [21], whereas free-space coupling first excites chaotic modes of the deformed cavity that then excite the high-Q modes though the dynamical tunneling.

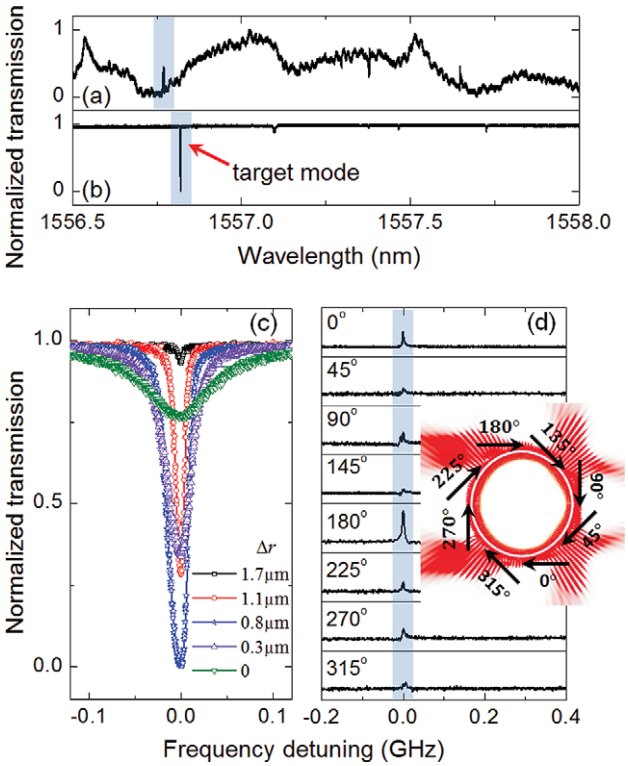

Figure 3 Comparison of the transmission spectra obtained with the focused beam excitation (a) and the fiber taper coupling (b). (c) The transmission spectra around the same resonance mode when coupled to the taper for different taper-cavity gaps. The blue curve shows the critical coupling case. (d) The transmission spectra around the target resonance mode for eight typical coupling positions of the focused beam shown in the inset.

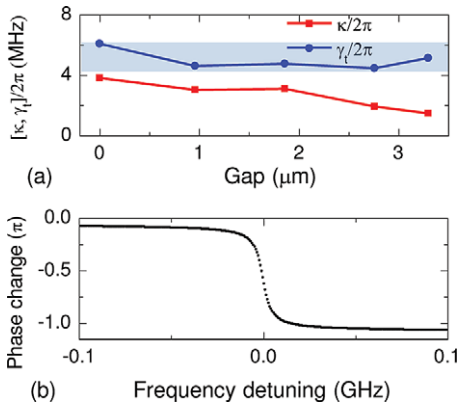

Figure 4 (a) Modeled κ and γ_t in Figs. 2(f)-2(j) depending on the beam-cavity gap. The shadow shows the measured linewidth range with a fiber taper coupling. (b) The calculated phase change of the transmitted field in Fig. 2(f), showing strong normal dispersion.

The transparency resonances using free-space coupling depend strongly on the excitation positions. As shown in Fig. 3(d), the highest transparency peak occurs when the incident beam focuses on the cavity edge at the polar position $\phi \sim \pi/2$ and from the 180° far-field direction (see the inset of Fig. 3(d)). This is the exact position where high-Q counter-clockwise resonances show the strongest directional emission assisted by chaos. By time-reversing this process, this is also where the chaotic modes are most strongly excited by the incident laser. In our experiment, the transmission spectra of a circular toroidal microcavity are also measured, devoid of chaotic modes, excited by a free-space laser, and no efficient coupling and Fano-like EIT resonance for a single resonant mode were observed. This further confirms that coupling with the chaotic modes in deformed microcavities is indeed responsible for the induced transparency.

To obtain more insight on the coupling features mentioned above, in what follows the experimental transmission spectra are theoretically modeled. In the free-space coupling process shown in Fig. 1(c), the incident light $|\mathrm{in}\rangle$ with frequency ω is scattered by the microcavity and directly excites continuous chaotic modes, denoting the excitation state $|\mathrm{C}_\omega\rangle$ [30]. We consider that a discrete regular quasi-mode $|\mathrm{M}\rangle$ with resonant frequency ω_0 interacts with the chaotic modes, and assume that the $|\mathrm{C}_\omega\rangle$ and $|\mathrm{M}\rangle$ are orthogonal and normalized [25, 32] before performing a perturbation treatment. The interacting system is governed by a Hamiltonian H, satisfying $\langle \mathrm{M}|H|\mathrm{M}\rangle = \omega_0 - i\gamma/2$, $\langle \mathrm{C}_\omega|H|\mathrm{M}\rangle = V_\omega$, and $\langle \mathrm{C}_{\omega'}|H|\mathrm{C}_\omega\rangle = \omega\delta(\omega' - \omega)$. Here V_ω describes the interaction between $|\mathrm{M}\rangle$ and $|\mathrm{C}_\omega\rangle$, known as the dynamical tunneling; γ represents the modified decay rate of $|\mathrm{M}\rangle$, consisting of (i) the intrinsic loss such as radiation, material absorption and scattering, and (ii) the tunneling into other chaotic states that are not directly excited by free-space coupling.

With a standard procedure developed by Fano in Ref. [31], the transmission spectrum of the free-space beam is obtained

$$T(\omega) = \frac{|q_\omega + \epsilon - iK|^2}{(1+K)^2 + \epsilon^2} T_0(\omega). \qquad (1)$$

Here K is defined as the ratio $\gamma/\kappa \equiv (\gamma_t - \kappa)/\kappa$ with $\kappa = 2\pi|V_\omega|^2$ being the coupling strength [33] and $\gamma_t \equiv \kappa + \gamma$ representing the whole decay rate of the regular mode; $\epsilon \equiv (\omega - \omega_0)/(\kappa/2)$ describes the detuning between the incident light and the regular mode; q_ω stands for the shape parameter of the Fano resonance; $T_0(\omega)$ describes the uncoupled scattering background (*i.e.*, $\kappa = 0$). In experiment, $T_0(\omega)$ can be obtained from a large-range wavelength scanning, which shows baseline oscillations resulting from the interference of two amplitudes: (i) the directly transmitted amplitude, and (ii) the dissipated amplitude that refracts into and back from the cavity.

Under this model, the red solid curves in Figs. 2(f)-2(j) show the theoretical fittings, in good accordance with the experimental spectra (blue dots). The fitting parameters $\kappa/2\pi$ and $\gamma_t/2\pi$ are plotted in Fig. 4(a). It can be seen that the coupling between the regular and the excitation states, described by the strength κ, becomes weaker when the focused beam moves away from the cavity boundary.

This is possibly due to the reduced direct refraction into the cavity and to the lower distribution of the excited $|C_\omega\rangle$ states in phase space. Furthermore, the modeled total decay rates $\gamma_t/2\pi$ of the high-Q mode, which is an invariant in our theory, range from 4 to 6 MHz, falling within the error of the measured resonant linewidth.

To characterize the induced transparency, Fig. 4(b) shows the calculated phase change of the transmitted field with the modeled data in Fig. 2(f). This conventional curve exhibits an extremely steep normal dispersion, and indicates a strong suppression of the group velocity. At the resonance point $\omega \sim \omega_0$, the group velocity is significantly reduced to smaller than $10^{-5}c$ where c is the velocity of light in vacuum, resulting from the ultra-narrow linewidth of the ultrahigh-Q resonance mode in the deformed microcavity.

In summary, we have experimentally demonstrated dynamical tunneling-induced transparency in a chaotic microcavity with a Q factor exceeding 3×10^7. When excited by a focused laser beam, the induced transparency in the transmission spectrum is attributed to the destructive interference of two optical pathways: one is to directly excite the continuous chaos from the incident beam, and the other excites the high-Q mode (by dynamical tunneling) coupling back to the chaos. By controlling the excitation position of the laser beam, the induced transparency experiences a highly tunable Fano-like asymmetric lineshape. This induced transparency is accompanied by extremely steep normal dispersion, which provides a dramatic slow light behavior and a significant enhancement of nonlinear interactions in an optical microcavity.

Acknowledgement. Y.F.X. thanks Kyungwon An, Kerry Vahala, and William Clements for stimulating discussions and suggestions. This work was supported by the 973 project (No. 2013CB328704), and NSFC (Nos. 11004003, 11222440, and 11121091). Q.F.Y. was supported by the National Fund for Fostering Talents of Basic Science (No. J1030310 and No. J1103205).

Received: 21 March 2013, **Revised:** 24 April 2013,
Accepted: 27 May 2013

Published online: 25 June 2013

Key words: Induced-transparency, chaotic microcavity, dynamical tunneling, fano resonance.

References

[1] K. J. Boller, A. Imamoglu, and S. E. Harris, Phys. Rev. Lett. **66**, 2593 (1991).
[2] M. Fleischhauer, A. Imamoglu, and J. P. Marangos, Rev. Mod. Phys. **77**, 633 (2005).
[3] S. E. Harris, Phys. Rev. Lett. **77**, 5357 (1996).
[4] R. Gad, J. G. Leopold, A. Fisher, D. R. Fredkin, and A. Ron, Phys. Rev. Lett. **108**, 155003 (2012).
[5] A. G. Litvak and M. D. Tokman, Phys. Rev. Lett. **88**, 095003 (2002).
[6] C. L. G. Alzar, M. A. G. Martinez, and P. Nussenzveig, Am. J. Phys. **70**, 37 (2002).
[7] D. D. Smith, H. Chang, K. A. Fuller, A. T. Rosenberger, and R. W. Boyd, Phys. Rev. A **69**, 063804 (2004).
[8] L. Maleki, A. B. Matsko, A. A. Savchenkov, and V. S. Ilchenko, Opt. Lett. **29**, 626 (2004).
[9] M. F. Yanik, W. Suh, Z. Wang, and S. Fan, Phys. Rev. Lett. **93**, 233903 (2004).
[10] K. Totsuka, N. Kobayashi, and M. Tomita, Phys. Rev. Lett. **98**, 213904 (2007).
[11] Q. Xu, P. Dong, and M. Lipson, Nature Phys. **3**, 406 (2007).
[12] N. Papasimakis, V. A. Fedotov, N. I. Zheludev, and S. L. Prosvirnin, Phys. Rev. Lett. **101**, 253903 (2008).
[13] P. Tassin, L. Zhang, Th. Koschny, E. N. Economou, and C. M. Soukoulis, Phys. Rev. Lett. **102**, 053901 (2009).
[14] A. H. Safavi-Naeini, T. P. Mayer Alegre, J. Chan, M. Eichenfield, M. Winger, Q. Lin, J. T. Hill, D. E. Chang, and O. Painter, Nature (London) **472**, 69 (2011).
[15] S. Weis, R. Rivière, S. Deléglise, E. Gavartin, O. Arcizet, A. Schliesser, T. J. Kippenberg, Science **330**, 1520 (2010).
[16] J. U. Nöckel and A. D. Stone, Nature (London) **385**, 45 (1997).
[17] C. Gmachl, F. Capasso, E. E. Narimanov, J. U. Nöckel, A. D. Stone, J. Faist, D. L. Sivco, and A. Y. Cho, Science **280**, 1556 (1998).
[18] S. Shinohara, T. Harayama, T. Fukushima, M. Hentschel, T. Sasaki, and E. E. Narimanov, Phys. Rev. Lett. **104**, 163902 (2010).
[19] Q. Song, L. Ge, B. Redding, and H. Cao, Phys. Rev. Lett. **108**, 243902 (2012).
[20] M. J. Davis and E. J. Heller, J. Chem. Phys. **75**, 246 (1981).
[21] D. K. Armani, T. J. Kippenberg, S. M. Spillane, and K. J. Vahala, Nature (London) **421**, 925 (2003).
[22] X.-F. Jiang, Y.-F. Xiao, C.-L. Zou, L. He, C.-H. Dong, B.-B. Li, Y. Li, F.-W. Sun, L. Yang, and Q. Gong, Adv. Mat. **24**, OP260 (2012).
[23] M. Hentschel, and K. Richter, Phys. Rev. E **66**, 056207 (2002).
[24] M. Soltani, Q. Li, S. Yegnanarayanan, and A. Adibi, Opt. Express **18**, 19541 (2010).
[25] J. Yang, S-B. Lee, S. Moon, S.-Y. Lee, S. W. Kim, T. T. A. Dao, J.-H. Lee, and K. An, Phys. Rev. Lett. **104**, 243601 (2010).
[26] Y. S. Park and H. Wang, Nature Physics **5**, 489 (2009).
[27] V. F. Lazutkin, KAM theory and semiclassical approximations to eigenfunctions (Springer, New York, 1993).
[28] J. Wiersig and M. Hentschel, Phys. Rev. Lett. **100**, 033901 (2008).
[29] J.-B. Shim, S.-B. Lee, S. W. Kim, S.-Y. Lee, J. Yang, S. Moon, J.-H. Lee, and K. An, Phys. Rev. Lett. **100**, 174102 (2008).
[30] Q.-F. Yang, X.-F. Jiang, Y.-L. Cui, L. Shao, and Y.-F. Xiao, http://arxiv.org/abs/1209.3395.
[31] U. Fano, Phys. Rev. **124**, 1866 (1961).
[32] P. T. Kristensen, C. V. Vlack, and S. Hughes, Opt. Lett. **37**, 1649 (2012).
[33] C. W. Gardiner and P. Zoller, Quantum Noise, 3rd ed. (Springer, Berlin, 2004).